Desalination and Water Treatment
www.deswater.com

doi: 10.5004/dwt.2021.27007

220 (2021) 421–430
April

Hyperbranched polysiloxane functionalized coal fly ash as an inexpensive adsorbent for removing malachite green

Mengmeng Zhang[a,*], Zhaojun He[b], Xin Chen[b]

[a]*State Key Laboratory of Nuclear Resources and Environment; School of Chemistry, Biology and Materials Science, East China University of Technology, Nanchang 330013, Jiangxi, China, email: zhangmengmeng0301@126.com*
[b]*School of Chemistry, Biology and Materials Science, East China University of Technology, Nanchang 330013, Jiangxi, China, emails: 1437343543@qq.com (Z. He), 371985348@qq.com (X. Chen)*

Received 6 November 2020; Accepted 4 January 2021

ABSTRACT

Hyperbranched polysiloxane functionalized coal fly ash (HP-CFA) was prepared via a facile hydrolytic condensation strategy. The HP-CFA was characterized using Fourier-transform infrared spectra, X-ray diffraction, thermogravimetric analysis, and scanning electron spectroscopy. The use of HP-CFA for the adsorption of malachite green from aqueous samples was studied in detail by varying the parameters including adsorbent amount, adsorption time, initial malachite green concentration, and temperature. Adsorption kinetics, adsorption isotherms, and adsorption thermodynamics were investigated to verify the nature and feasibility of the adsorption of malachite green onto HP-CFA. The adsorption kinetics were in well-accordance with the pseudo-second-order model as the correlation coefficient values were all over 0.99. The experimental isotherms were better represented by the Langmuir model than the Freundlich model. Thermodynamic calculation results indicated that the adsorption occurred spontaneously and endothermically. The regeneration study showed that the adsorption capability of HP-CFA toward malachite green after five-time cycles was maintained about 78% of the original adsorption capacity. Overall, this work suggests the HP-CFA is promising to be applied as an inexpensive and efficient adsorbent in applicable removal of dyes in wastewater.

Keywords: Fly ash; Hyperbranched polysiloxane; Removal; Malachite green

1. Introduction

Dyes and pigments are widely used in many industries such as textile, leather, paper, and food colorings. Discharge of these dyes sewage into waters poses severe threats to the environment because of the toxic nature and suspected carcinogenic, mutagenic, and neurotoxic effects of synthetic dyes on aquatic lives and humans [1–4]. Malachite green, a triphenylmethane dye, is usually applied in the dyeing of wool, leather, paper, silk, and cotton. It is also utilized as a bactericide in the aquaculture industry for treating fungal, parasitic, and bacterial infections in fish. However, malachite green has been found to be a possibly cancer-causing chemical and it possesses high toxicity, refractory, and mutagenicity to animals and human beings [5,6]. The available toxicological observations on malachite green indicate that it is a multi-organ toxin. It can cause injury to the eyes, skins, and bones, and damage to the lungs, heart, spleen, liver, kidney, and brain. In the tissues of aquatic animals, malachite green can be rapidly reduced into leuco-malachite green, which is also a highly toxic material and has carcinogenic effects. Moreover, there are reports that the degradation products

---

[*] Corresponding author.

1944-3994/1944-3986

of malachite green are also not safe and can cause pollution to the environment [7–9]. Though the use of malachite green in aquaculture has been banned in many countries, it is still being used in many countries because of its low cost and high effectiveness for saprolegniasis treatment. Therefore, it is imperative to remove malachite green from wastewater to prevent its harmful impacts on aquatic ecosystems.

Various techniques, such as micro-electrolysis, chemical oxidation, adsorption, magnetic separation, ultrasonic degradation, and physical–chemical–biological method have been applied in the purification of dye wastewater [10–15]. Adsorption is recognized as one of the most efficient ways of eliminating pollutants for various reasons. Generally, the adsorption technique possesses high flexibility, efficiency, and simplicity in design, which provides the possibility of trying different kinds of natural and synthetic adsorbents [16–18]. Large amounts of adsorption materials have been applied for removing dyes from water such as silica gel, molecular sieve, biomass carbon material, magnetic nanomaterials, and porous polymers, etc., [19–23]. The materials used for adsorption should possess the following properties: large adsorption capacity, high stability, good reusability, high safety in use, favorable environmental protection, and convenient operation [24,25]. So far, the design and manufacture of economical, efficient, and environment-friendly adsorbents is still a challenge in the industrial applications of the adsorption technique. Coal fly ash (CFA), a solid waste generated from coal-fired power plants, is produced in huge amount every year. CFA usually possesses hollow spheres and activated sites, showing a good prospect for its adsorption application. Whereas, the original CFA usually exhibits low adsorption capacity, so physical and chemical methods are generally applied to modify CFA to improve its adsorption capacity. Zhang et al. [26] synthesized CFA/$CoFe_2O_4$ composites via a facile hydrothermal method. The CFA/$CoFe_2O_4$ magnetic composites was proved to be an efficient adsorbent for adsorption of malachite green from the aqueous sample with a maximum adsorption capacity of 89.3 mg/g. Visa and Chelaru [27] adopted NaOH and hexadecyltrimethylammonium bromide to modify CFA for removing heavy metals and dyes. Gao et al. [28] reported that CFA modified by $Ca(OH)_2/Na_2FeO_4$ could be applied to remove methyl orange from water, and the maximum adsorption capacity was 14.76 mg/g. Dash et al. [29] investigated the adsorption property of CFA functionalized with polyethyleneimine toward cationic and anionic dyes. The results showed that the adsorption capacity of the adsorbent on the malachite green was significantly higher than that of the raw CFA. These modified CFAs were proved to be efficient adsorbents for dye removal from the aqueous phase. However, large-scale applications of these modified CFAs are still restricted because of the relatively high cost of modification, low regeneration capability, and secondary pollution caused by the modification process. Therefore, it is necessary to develop inexpensive and facile methods to modify CFA to enhance its adsorption property and reusability.

Hyperbranched polysiloxane is a kind of polymer with a highly branched three-dimensional structure, which combines the advantages of both hyperbranched polymers and polysiloxanes [30,31]. In comparison with linear polysiloxanes, hyperbranched polysiloxanes possess a considerably higher density of functional groups, higher branching degree, and better stability [32,33]. Additionally, hyperbranched polysiloxanes possess many unoccupied cavities, which can encapsulate organic pollutants and metal ions [34,35]. Therefore, in order to enhance the adsorption properties of CFA, hyperbranched polysiloxanes functionalized CFA may be an effective method for achieving satisfactory adsorption performance. To the best of our knowledge, there are few literatures focused on the removal of dyes using CFA functionalized with hyperbranched polysiloxanes. Herein, the CFA was functionalized by a hyperbranched polysiloxane via a hydrolytic condensation method, then the functionalized CFA was used as an adsorbent for malachite green removal in an aqueous solution. This CFA functionalization method is cheap, facile, and effective, which can not only greatly enhance the adsorption property of CFA, but also cause no secondary pollution, showing a promising industrial application prospect in the water-remediation field.

2. Materials and methods

2.1. Chemicals

CFA powders were provided by Shaanxi Zhengdao Environmental Protection Building Materials Co., Ltd., (Shaanxi, China). Malachite green was purchased from Shanghai Meryer Chemical Technology Co., Ltd., (Shanghai, China). γ-Aminopropyltriethoxysilane (KH-550) was purchased from Shanghai Macklin Biochemical Technology Co., Ltd., (Shanghai, China). Sodium hydroxide (NaOH) was purchased from Sinopharm Chemical Reagent Co., Ltd., (Beijing, China). Ethanol was purchased from Wanlianda Chemical Co., Ltd., (Tianjin, China).

2.2. Functionalization of CFA by hyperbranched polysiloxane

0.5 g of CFA, 70 mL of ethanol, and 1.0 mL of distilled water were mixed together in a 250 mL three-mouth flask, and then ultrasound dispersed for 30 min to form a homogeneous suspension. The flask was then placed in a water bath to heated up to 30°C with mechanical stirring. Then a mixture of KH-550 (10 mL) and ethanol (20.0 mL) was added drop-wise into the flask. The temperature was raised up to 75°C and kept for 5–7 h with stirring. After the reaction, the suspension was washed using ethanol and distilled water for several times. The obtained black powder is dried in a vacuum oven at 60°C for 12 h. The final product obtained is referred to in this study as hyperbranched polysiloxane functionalized CFA (HP-CFA). The synthetic route of HP-CFA is shown in Fig. 1.

2.3. Characterization

Fourier transform infrared (FT-IR) spectra of CFA and HP-CFA are examined by a Nicolet 5700 infrared spectrometer (Nicolet, USA) from 400 to 4,000 cm^{-1}.

X-ray diffraction (XRD) patterns of CFA and HP-CFA are recorded on a PANalytical X'Pert X-ray diffractometer (PANalytical, Holland) using Cu Kα (λ = 0.154 nm) radiation.

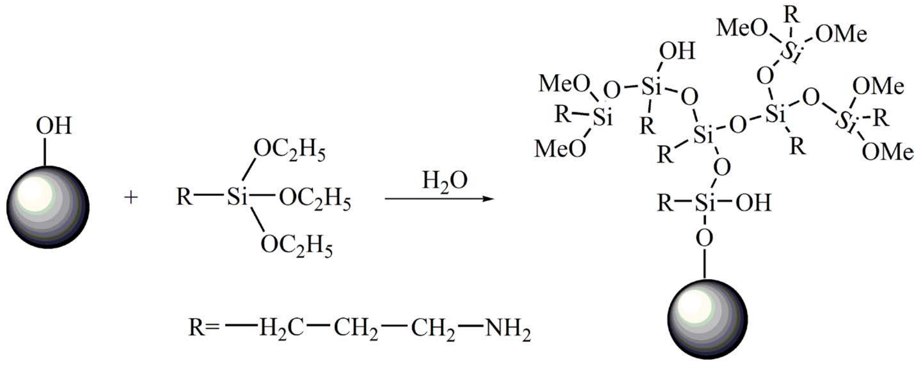

Fig. 1. Synthetic route of HP-CFA.

The tests are performed at an ambient temperature with a scanning rate of 0.02°/s.

Thermogravimetric analyses (TGA) of CFA and HP-CFA are performed on a ZRT-B thermogravimetric analyzer in a nitrogen atmosphere at a heating rate of 20°C/min.

The surface morphologies of CFA and HP-CFA are characterized using field emission scanning electronic microscopy (SEM, TESCAN CLARA, Czech Republic).

2.4. Adsorption experiments

Generally, a certain amount of HP-CFA powder and 50 mL malachite green solution were mixed in a 250 mL conical flask. The conical flask was then kept in a constant temperature water bath oscillator and shaken for a certain time. After the adsorption, the used HP-CFA was separated by filtration. The residual malachite green left in the solution was measured by a UV-vis spectrophotometer at λ of 616.9 nm. The removing efficiency (R) and instantaneous adsorption capacity (q_t) of malachite green on HP-CFA are evaluated using equations as cited by Soni et al. [36].

2.5. Reusability of HP-CFA

The desorption of HP-CFA was studied using a sodium hydroxide solution (0.1 mol/L) as eluent. Firstly, 0.095 g of HP-CFA was immersed into 50 mL of 240 mg/L malachite green solutions and the mixture was shaken at ambient temperature for 90 min. Then the used HP-CFA was removed from the malachite green solution by filtering. The obtained powder was placed in 50 mL of sodium hydroxide solution (0.1 mol/L), followed by vigorous oscillation for 60 min. Then the regenerated HP-CFA was removed from the solution and washed with water. The recovered HP-CFA was reused in adsorption experiments to measure its recyclability.

3. Results and discussions

3.1. FT-IR analysis of HP-CFA

FT-IR analysis was performed to examine the functional groups on the surface of CFA and HP-CFA. The FT-IR spectrum of raw CFA is shown in Fig. 2a. The characteristic peak at 3,440 cm^{-1} is attributed to the stretching vibration of the hydroxyl group. Peak located at 1,071 cm^{-1} is generated by the Si–O–Si bond. The peak is shown at 470 cm^{-1} is ascribed to the bending mode of O–Si–O. These characteristic peaks indicate that the main oxide constituent in CFA is silicon dioxide. Fig. 2b presents the FT-IR spectrum of HP-CFA. Peaks appearing at 2,924 and 2,853 cm^{-1} are generated by –CH_3 and –CH_2– stretching vibrations, respectively. It is obvious that the peak intensity at 1,071 cm^{-1} in Fig. 2b is much higher than that of raw CFA, which is attributed to the Si–O–Si stretching vibration of hyperbranched polysiloxane.

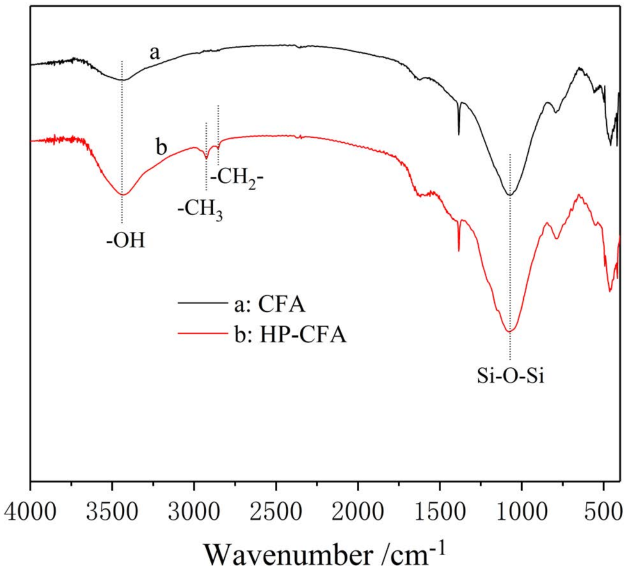

Fig. 2. FTIR spectra of CFA (a) and HP-CFA (b).

3.2. XRD analysis of HP-CFA

The XRD patterns of CFA and HP-CFA were collected in the 2θ range of 5°–80° to examine the differences before and after the functionalization. The raw CFA (Fig. 3a) shows a sharp diffraction peak at 2θ° = 26.6°, which indicates the presence of mullite and quartz in the original CFA. In the case of HP-CFA (Fig. 3b), there are no obvious changes in the XRD spectrum after surface functionalization with hyperbranched polysiloxane, suggesting that the

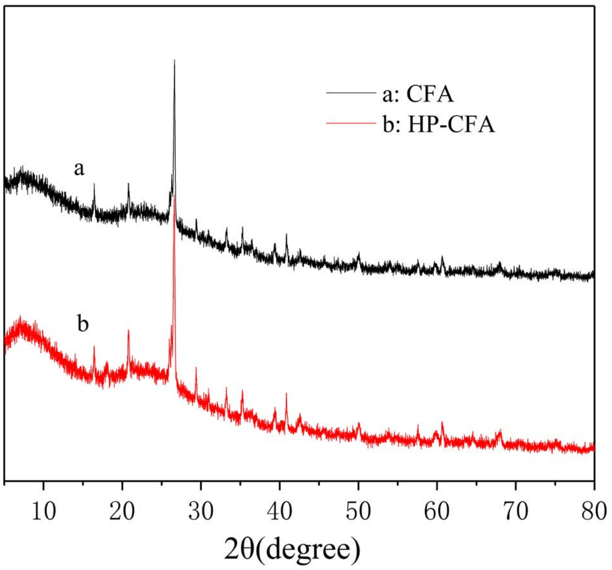

Fig. 3. XRD patterns of CFA (a) and HP-CFA (b).

surface functionalization has an insignificant influence on the crystal structure of CFA.

3.3. *Thermogravimetric analysis of HP-CFA*

Thermal stabilities of CFA and HP-CFA are evaluated by thermogravimetric analysis (TGA). Fig. 4 presents the TGA curves of raw CFA and HP-CFA. From Fig. 4a, CFA is hardly decomposed before 150°C, and only 2.2% weight loss can be observed at 900°C, revealing the good thermally stability of raw CFA. From Fig. 4b, the weight loss of HP-CFA is higher than that of CFA because the functional groups on HP-CFA is thermally unstable. The weight loss of 1.1% between 25°C and 150°C is assigned to the presence of absorbed water. A significant weight loss that occurred between 150°C and 900°C is calculated about 11.2%, which is caused by the thermal decomposition of the hyperbranched polysiloxane.

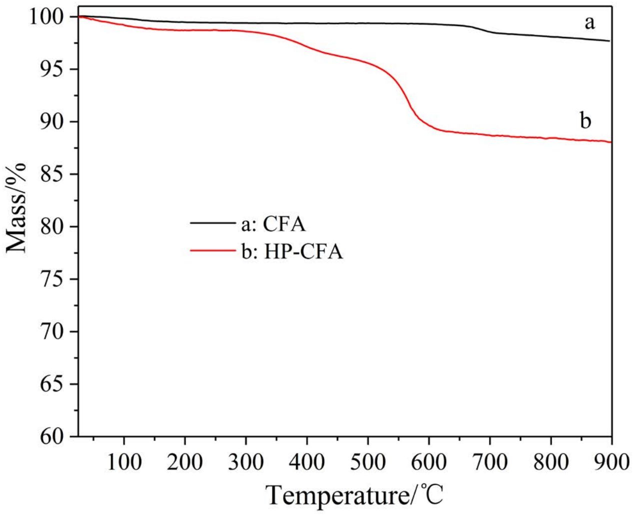

Fig. 4. TGA curves of CFA (a) and HP-CFA (b).

3.4. *SEM of HP-CFA*

The microstructural-level details of CFA and HP-CFA are recorded by SEM, and the obtained micrographs are shown in Fig. 5. The raw CFA (Fig. 5a) exhibits a morphology of spherical particles with relatively uniform and smooth surfaces. Whereas the surface of HP-CFA (Fig. 5b) are much rougher, and many flocs are deposited on the surface of spherical particles, indicating the presence of hyperbranched polysiloxane on the CFA surface.

3.5. *Effect of adsorbent amount*

The effect of HP-CFA amount on the removal efficiency and adsorption capacity of malachite green was evaluated by varying the HP-CFA amount used for adsorption from 0.05 to 1.0 g with an initial malachite green solution concentration of 120 mg/L. Fig. 6 shows that there is a positive correlation between the removal efficiency of malachite green and the dosage of HP-CFA. The removal

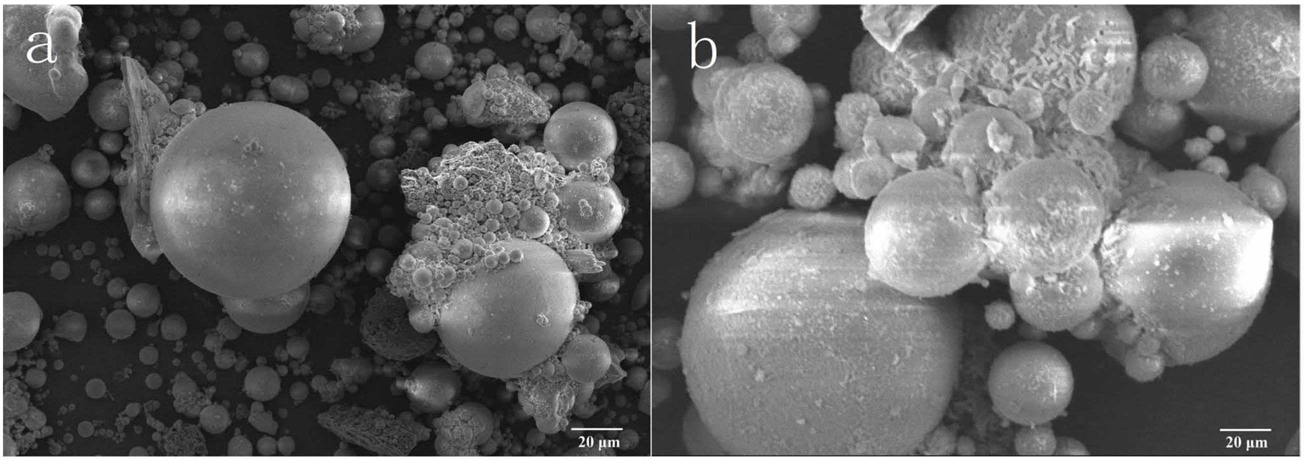

Fig. 5. SEM images of CFA (a) and HP-CFA (b).

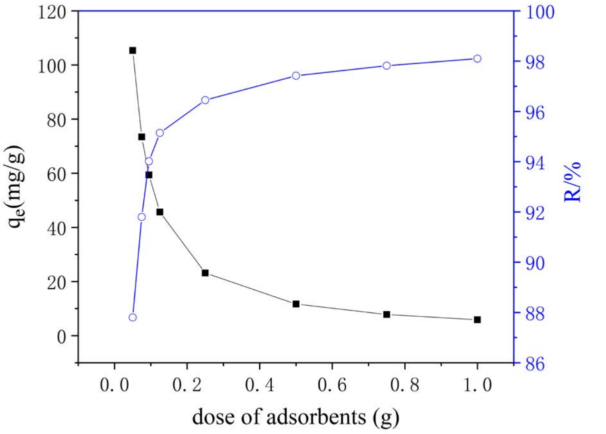

Fig. 6. Effect of HP-CFA amount on adsorption capacity and removal efficiency of malachite green onto HP-CFA.

efficiency of the malachite green increases from 87.8% to 94.0% by increasing the amount of adsorbent from 0.05 to 0.095 g, which is due to the fact that the increased amount of HP-CFA can provide more available adsorption sites for the adsorption of malachite green. With a further increase in the amount of HP-CFA, no obvious enhancement in the removing efficiency is observed. On the contrary, there is a significant decrease in the adsorption capacity of malachite green from 105.4 to 5.9 mg/g when the adsorption dosage increases from 0.05 to 1 g. The decrease of adsorption capacity is attributed to the fact that more adsorbents will lead to unsaturated adsorption sites, thus resulting in a lower adsorption capacity value. Considering the two aspects of cost and efficiency of the adsorbent, 0.095 g of HP-CFA was used in the subsequent experiments.

3.6. Effect of adsorption time

The effect of adsorption time on malachite green adsorption capacity on HP-CFA is examined at three different initial malachite green concentrations of 120, 180, and 240 mg/L, and the results are outlined in Fig. 7. Within incipiently 30 min, the adsorption capacity of malachite green rapidly increases. At the initial stage of adsorption, there are a large number of vacant adsorption sites on the surface of HP-CFA and it is easy for malachite green molecules to combine these adsorption sites. With the further increase of adsorption time, the adsorption capacity of malachite green increases slowly and gradually tends to achieve a steady value. The adsorption equilibrium is reached at about 90 min, and the adsorption equilibrium time is longer when the initial concentration is higher. The decrease in adsorption rate is attributed to the decrease of vacant adsorption sites. In addition, it is also noted that the equilibrium adsorption capacity increases along with the increase of initial malachite green concentration, which is due to the higher driving force for mass transfer at a higher initial dye concentration.

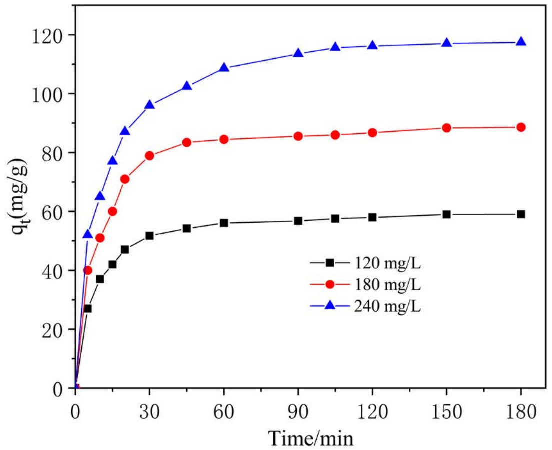

Fig. 7. Effect of adsorption time on adsorption capacity of malachite green onto HP-CFA.

3.7. Effect of the initial concentration of malachite green and temperature

The effect of the initial concentration of malachite green on the adsorption capacity at various temperatures is investigated by conducting the adsorption experiment with a wide range of initial malachite green concentration from 60 to 270 mg/L, and the results are outlined in Fig. 8. The adsorption capacity of malachite green markedly increases with the increasing of initial malachite green concentration, and an adsorption equilibrium trends to reach when the initial dye concentration exceeds 240 mg/L. The maximum adsorption amount of malachite green on HP-CFA with the initial dye concentration of 270 mg/L at 25°C is 119 mg/g. The high adsorption capability might be attributed to the following two reasons, as illustrated in Fig. 9. Firstly, the introduced amino groups on the HP-CFA surface can easily combine with adsorbates through hydrogen bonding. Secondly, the hyperbranched polysiloxane possesses many unoccupied cavities that can encapsulate dye molecules, thus promoting the adsorption of malachite green onto HP-CFA. In addition, from Fig. 8, there is little difference in the adsorption capacities of malachite green on HP-CFA at the three different temperatures, implying that temperature is not the main factor affecting the adsorption process of malachite green onto HP-CFA.

3.8. Adsorption kinetic studies

Adsorption kinetic studies can give an insight into the rate-limiting step and plausible adsorption mechanism. In this paper, the experimental data are simulated using two conventional adsorption kinetic models (pseudo-first-order and pseudo-second-order models). The linear forms of pseudo-first-order and pseudo-second-order models can be represented as Eqs. (1) and (2), respectively:

$$\log\left(q_e - q_t\right) = \log q_e - k_1 \frac{t}{2.303} \tag{1}$$

$$\frac{t}{q_t} = \frac{1}{k_2 q_e^2} + \frac{t}{q_e} \tag{2}$$

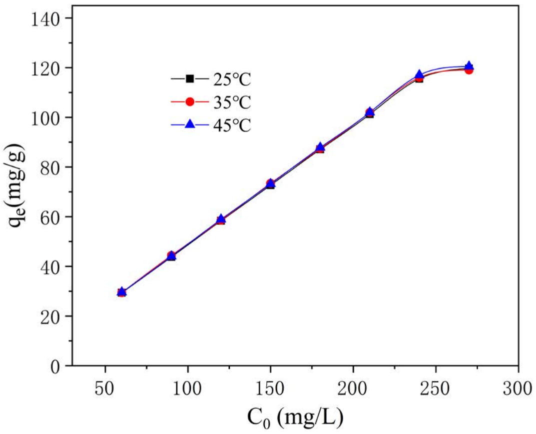

Fig. 8. Effect of initial malachite green concentration and temperature on adsorption capacity of malachite green onto HP-CFA.

where q_e and q_t (mg/g) represent the adsorption capacity of malachite green at equilibrium and at adsorption time t (min), respectively. k_1 (min^{-1}) is the pseudo-first-order rate constant. k_2 (g/mg min) is the pseudo-second-order rate constant. The adsorption kinetics curves simulated by the pseudo-first-order and pseudo-second-order models are shown in Figs. 10 and 11, respectively. The related kinetic fitting parameters and correlation coefficients (R^2) obtained from the above two fitting curves are presented in Table 1. According to the results, the curves fitted by pseudo-first-order model at three different initial dye concentrations all exhibit relatively low R^2 values (0.6936–0.9236), and the $q_{e,\text{cal}}$ (mg/g) values obtained from the pseudo-first-order model are markedly different from the experimental values of $q_{e,\text{exp}}$ (mg/g), suggesting that the pseudo-first-order model is not suitable for describing the adsorption behavior of malachite green onto HP-CFA. In contrast, the R^2 values obtained from the pseudo-second-order model at three different initial dye concentrations all exceed 0.99. Moreover, the $q_{e,\text{cal}}$ (mg/g) values obtained from the pseudo-second-order model are very close to the experimentally measured adsorption capacity values. These results imply that the adsorption kinetics of malachite green onto HP-CFA are well-consistent with the pseudo-second-order model.

3.9. Adsorption isotherm studies

The adsorption mechanism and interactions between adsorbent surfaces and adsorbates can be acquired from adsorption isotherm studies. Two commonly used isotherm models, namely, Langmuir and Freundlich adsorption isotherm models are applied to describe the adsorption behavior of malachite green onto HP-CFA. The linear form of Langmuir and Freundlich models can be expressed as Eqs. (3) and (4), respectively:

$$\frac{C_e}{q_e} = \frac{C_e}{q_m} + \frac{1}{K_L q_m} \tag{3}$$

$$\ln q_e = \ln K_F + \frac{1}{n} \ln C_e \tag{4}$$

where C_e (mg/L) represents the adsorption equilibrium concentration of malachite green in solution. q_e (mg/g) represents the adsorption capacity of malachite green at equilibrium. $q_{\max}$ (mg/g) represents the theoretical maximum adsorption capacity of malachite green. K_L (L/mg) is the equilibrium constant from the Langmuir model, which is related to the binding energy and affinity of active sites in adsorption. K_F (mg/g (mg/L)$^{1/n}$) and $1/n$ are equilibrium constants from the Freundlich model associated with adsorption capacity and surface heterogeneity, respectively. The Langmuir model assumes that the adsorption process is based on the monolayer adsorption, and the surface of adsorbents are homogenous. Every adsorbent molecule in the solution is independent and has no interference with each other. The Freundlich model assumes that the multilayer adsorption occurs on the heterogeneous surface of the adsorbent, and there are interactions between the adsorbent molecules. The liner adsorption isotherm curves fitted by the Langmuir and Freundlich models are shown in Figs. 12 and 13, respectively. The R^2 values and relative isotherm constants evaluated from the above two isotherms are outlined in Table 2. The R^2 values obtained from the Langmuir isotherm model are 0.9858, 0.9901, and 0.9892 at 25°C, 35°C, and 45°C, respectively. While the R^2 values obtained from Freundlich models are 0.7821–0.8293, which are much smaller than the corresponding values from the Langmuir model. Therefore, the Langmuir model is a better

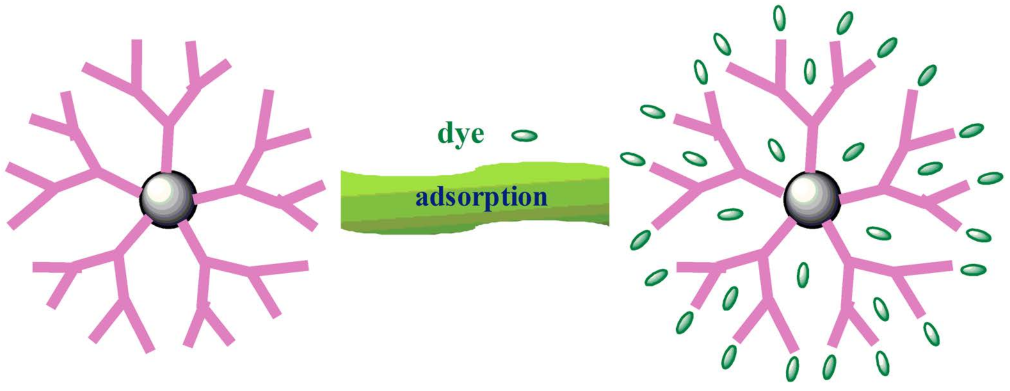

Fig. 9. Possible adsorption mechanism of malachite green by HP-CFA.

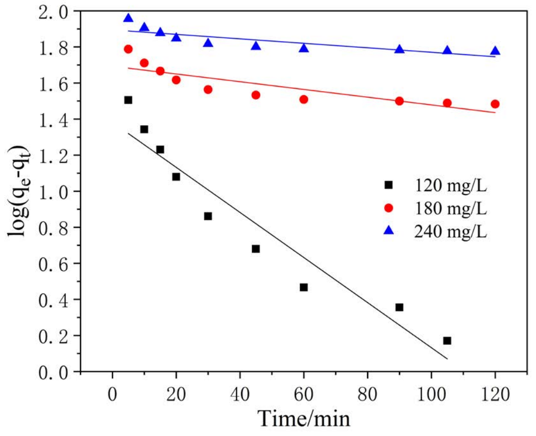

Fig. 10. Pseudo-first-order kinetic model for malachite green adsorption onto HP-CFA.

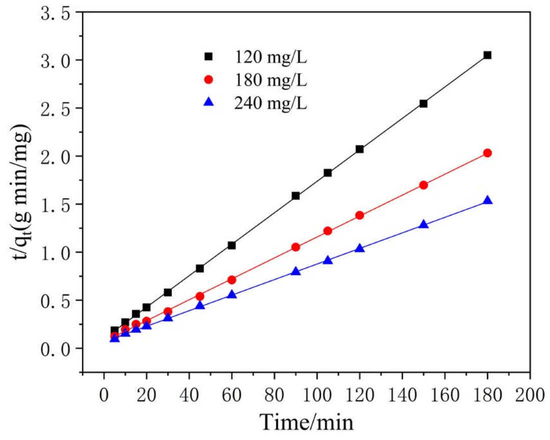

Fig. 11. Pseudo-second-order kinetic model for malachite green adsorption onto HP-CFA.

Table 1
Kinetic parameters of pseudo-first-order and pseudo-second-order models for malachite green adsorption onto HP-CFA

Kinetic models	Malachite green concentration (mg/L)		
	120	180	240
Pseudo-first-order			
$q_{e,\mathrm{exp}}$ (mg/g)	59.0160	88.603	117.4
$q_{e,\mathrm{cal}}$ (mg/g)	24.123	49.304	78.440
k_1 (min^{-1})	0.2904	0.0049	0.0029
R^2	0.9236	0.7225	0.6936
Pseudo-second-order			
$q_{e,\mathrm{cal}}$ (mg/g)	60.97	90.90	121.45679
k_2 (g/mg·min)	0.00258	0.00175	0.00101
R^2	0.9999	0.9997	0.9998

fit for describing the adsorption isotherm, implying the adsorption of malachite green on HP-CFA is mono-layer adsorption. The theoretical q_m values calculated from the Langmuir model are 135.7, 131.9, and 133.0 mg/g at 25°C, 35°C, and 45°C, respectively.

3.10. Thermodynamic studies

The mechanism and feasibility of the adsorption can be further explored by the thermodynamic study. Four parameters, including thermodynamic equilibrium constant (K_c), entropy change ($\Delta S°$), enthalpy change ($\Delta H°$), and Gibbs free energy change ($\Delta G°$) of the adsorption process can be obtained from Eqs. (5)–(7):

$$K_c = \frac{q_e}{C_e} \tag{5}$$

$$\ln K_c = \frac{\Delta S°}{R} - \frac{\Delta H°}{RT} \tag{6}$$

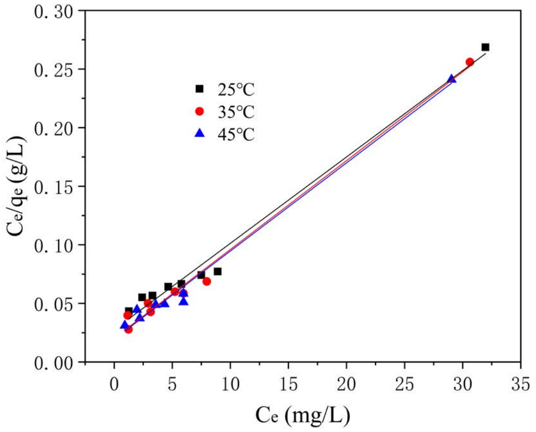

Fig. 12. Langmuir isotherm model for malachite green adsorption onto HP-CFA.

$$\Delta G° = \Delta H° - T\Delta S° \tag{7}$$

where C_e (mg/L) is the adsorption equilibrium concentration of malachite green in solution. q_e (mg/g) is the adsorption capacity of malachite green at equilibrium. R (8.314 J/mol K) is the universal gas constant. T (K) is the temperature. The values of $\Delta S°$ and $\Delta H°$ can be acquired from the slope and intercept of the plot of lnK_c vs. 1/T (figure omitted). By putting the values of $\Delta S°$ and $\Delta H°$ into Eq. (9), the values of $\Delta G°$ can be calculated. The calculated $\Delta G°$ values are –3.251, –3.503, and –3.775 kJ/mol at 298, 308, and 318 K, respectively. The calculated $\Delta H°$ and $\Delta S°$ values are 4.268 kJ/mol and 25.2321 J/mol K, respectively. The values of $\Delta G°$ at three different temperatures are all negative, confirming that the adsorption of malachite green on HP-CFA is feasible. The positive $\Delta S°$ value indicates an increase in randomness and disorder in adsorption. The positive $\Delta H°$ value suggests the endothermic nature of the adsorption process. Additionally, a gradual increase in the absolute value of $\Delta G°$ with the increasing temperature is noticed, which shows the enhancement in the spontaneity of adsorption at a higher temperature.

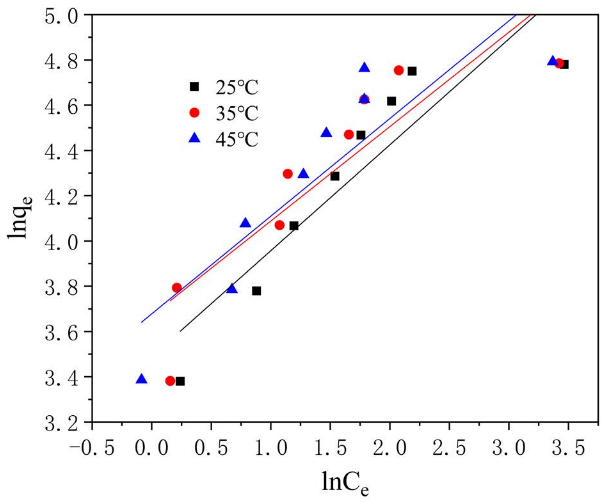

Fig. 13. Freundlich isotherm model for malachite green adsorption onto HP-CFA.

Table 2
Isotherm parameters of Langmuir and Freundlich models for malachite green adsorption onto HP-CFA

Isotherm models	Temperature (°C)		
	25	35	45
Langmuir			
q_m (mg/g)	135.69	131.93	132.98
K_L (L/mg)	0.2676	0.3752	0.3864
R^2	0.9858	0.9901	0.9892
Freundlich			
K_F (mg/g (mg/L)$^{1/n}$)	32.7437	39.2794	39.5612
$1/n$	0.468	0.4172	0.43152
R^2	0.8293	0.7958	0.7821

3.11. Recycling of HP-CFA

In order to assess the reusability and potential practical applications of HP-CFA, the desorption–adsorption experiments were conducted using 0.1 mol/L sodium hydroxide solution as strippant, and the results from the adsorption of malachite green upon recycling the HP-CFA for several cycles are presented in Fig. 14. A gradual decreasing tendency in the adsorption capacity with the increasing recycling times is noticed, which might be associated with the incomplete desorption of dye molecules in the desorption process. The adsorption capacity of HP-CFA toward malachite green is 91.7 mg/g after five-time cycles, which retains about 78% of the original adsorption capacity, showing that HP-CFA is appropriate for practical application as an inexpensive and recyclable adsorbent for malachite green removal.

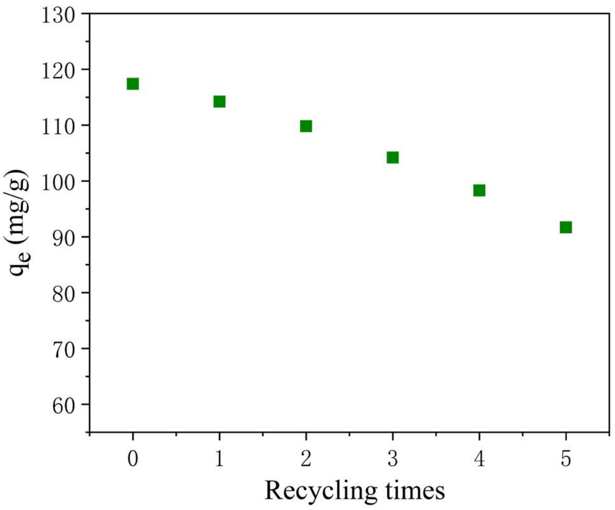

Fig. 14. Adsorption capacity of malachite green on HP-CFA over five-time adsorption–desorption cycles.

Table 3
Comparison of malachite green adsorption capacity of HP-CFA with other reported adsorbents

Adsorbents	q (mg/g)	T (°C)	References
HP-CFA	119.7	25	This work
Coal fly ash/$CoFe_2O_4$	89.3	25	[26]
$Ca(OH)_2$-treated fly ash	17.38	30	[28]
Fly ash microspherical particles	40.65	25	[37]
Activated carbon	27.44	30	[38]
Activated carbon/$CoFe_2O_4$	89.29	30	[39]
Sea shell powder	42.33	30	[40]
Graphite oxide/polyurethane foam	68.82	50	[41]
Forestry waste mixture	52.6	25	[42]
Chitosan ionic liquid beads	8.07	25	[43]
Carbon nanotubes	417.6	25	[44]
Amino-functionalized metal-organic framework (MOFs)	274.4	25	[45]
Copper sulfide nanorods loaded on activated carbon (CuS-NRs-AC)	145.98	25	[46]

3.12. Comparison of adsorption capacity of HP-CFA with other reported adsorbents on malachite green

The comparison of malachite green removal by HP-CFA with other adsorbents reported in the literatures is outlined in Table 3. The adsorption capacity of malachite green on HP-CFA is above average among the various adsorbents. The carbon nanotubes, MOFs, and CuS-NRs-AC represent higher adsorption capacity in comparison with HP-CFA. However, the adsorption capacity of malachite green on HP-CFA is superior to the activated carbon, seashell powder, graphite oxide composites, forestry waste mixture, and chitosan ionic liquid beads. Considering the effectiveness and cost, HP-CFA is a good candidate for practical applications in dye removal.

4. Conclusions

CFA functionalized with hyperbranched polysiloxane via a facile hydrolytic condensation method was demonstrated in this study. FT-IR, XRD, TGA, and SEM analysis confirmed the successful functionalization. The adsorption of malachite green from aqueous samples was affected by several parameters including HP-CFA amount, adsorption time, and initial malachite green concentration. Adsorption kinetic studies showed that experimental data matched to pseudo-second-order model with the high correlation coefficients (>0.99). Adsorption isotherm studies showed that the malachite green adsorption onto HP-CFA was better explained by the Langmuir model than the Freundlich model, and the theoretical maximum adsorption capacity at room temperature obtained from the Langmuir model was 135.7 mg/g. Thermodynamic parameters, including $\Delta S°$, $\Delta H°$, and $\Delta G°$ were calculated, and the results indicate the malachite green adsorption onto HP-CFA was a spontaneous, endothermic, and increasingly random process. Furthermore, the regeneration and reusability experiments also revealed the good sustainability of HP-CFA. Therefore, the economical, effective, and reusable functionalized CFA is expected to be applicable in the purification of dyestuff wastewater.

Acknowledgments

We acknowledge the financial support of Doctoral Research Start-up Fund Project of East China University of Technology (DHBK2017165).

References

[1] H. Anwer, A. Mahmood, J. Lee, K.H. Kim, J.W. Park, A.C.K. Yip, Photocatalysts for degradation of dyes in industrial effluents: opportunities and challenges, Nano Res., 12 (2019) 955–972.

[2] M. Wawrzkiewicz, E. Polska-Adach, Z. Hubicki, Application of titania based adsorbent for removal of acid, reactive and direct dyes from textile effluents, Adsorption, 25 (2019) 621–630.

[3] A. Hussein, M. Scholz, Dye wastewater treatment by vertical-flow constructed wetlands, Ecol. Eng., 101 (2017) 28–38.

[4] J. Mittal, Permissible synthetic food dyes in India, Resonance, 25 (2020) 567–577.

[5] S. Srivastava, R. Sinha, D. Roy, Toxicological effects of malachite green, Aquat. Toxicol., 66 (2004) 319–329.

[6] A. Mittal, L. Krishnan, V.K. Gupta, Removal and recovery of malachite green from wastewater using an agricultural waste material, de-oiled soya, Sep. Purif. Technol., 43 (2005) 125–133.

[7] V.K. Gupta, A. Mittal, L. Krishnan, V. Gajbe, Adsorption kinetics and column operations for the removal and recovery of malachite green from wastewater using bottom ash, Sep. Purif. Technol., 40 (2004) 87–96.

[8] A. Mittal, Adsorption kinetics of removal of a toxic dye, Malachite Green, from wastewater by using hen feathers, J. Hazard. Mater., 133 (2006) 196–202.

[9] C. Arora, P. Kumar, S. Soni, J. Mittal, A. Mittal, B. Singh, Efficient removal of malachite green dye from aqueous solution using *Curcuma caesia* based activated carbon, Desal. Water Treat., 195 (2020) 341–352.

[10] R. Xie, M. Wu, G. Qu, P. Ning, Y. Cai, P. Lv, Treatment of coking wastewater by a novel electric assisted micro-electrolysis filter, J. Environ. Sci., 66 (2017) 168–175.

[11] H. Shi, J. Li, D. Shi, H.J. Shi, B. Feng, W. Li, Y.P. Bai, J. Zhao, A.H. He, Combined reduction/precipitation, chemical oxidation, and biological aerated filter processes for treatment of electroplating wastewater, Sep. Sci. Technol., 50 (2015) 2303–2310.

[12] C. Arora, S. Soni, S. Sahu, J. Mittal, P. Kumar, P.K. Bajpai, Iron based metal organic framework for efficient removal of methylene blue dye from industrial waste, J. Mol. Liq., 284 (2019) 343–352.

[13] M. Fang, F. Mishima, Y. Akiyama, S. Nishijima, Fundamental study on magnetic separation of organic dyes in wastewater, Physica C, 470 (2010) 1827–1830.

[14] B.M. Jun, J. Han, C.M. Park, Y. Yoon, Ultrasonic degradation of selected dyes using $Ti_3C_2T_x$ MXene as a sonocatalyst, Ultrason. Sonochem., 64 (2020) 104993 (1–8), doi: 10.1016/j.ultsonch.2020.104993.

[15] G. Lofrano, S. Meric, G.E. Zengin, D. Orhon, Chemical and biological treatment technologies for leather tannery chemicals and wastewaters: a review, Sci. Total Environ., 461–462 (2013) 265–281.

[16] I. Anastopoulos, A. Mittal, M. Usman, J. Mittal, G. Yu, A. Núñez-Delgado, M. Kornaros, A review on halloysite-based adsorbents to remove pollutants in water and wastewater, J. Mol. Liq., 269 (2018) 855–868.

[17] V. Kumar, P. Saharan, A.K. Sharma, A. Umar, I. Kaushal, A. Mittal, Y. Al-Hadeethi, B. Rashad, Silver doped manganese oxide-carbon nanotube nanocomposite for enhanced dye-sequestration: Isotherm studies and RSM modelling approach, Ceram. Int., 46 (2020) 10309–10319.

[18] V.K. Gupta, S. Agarwal, R. Ahmad, A. Mirza, J. Mittal, Sequestration of toxic congo red dye from aqueous solution using ecofriendly guar gum/activated carbon nanocomposite, Int. J. Biol. Macromol., 158 (2020) 1310–1318.

[19] A.B. Volikov, S.A. Ponomarenko, A.I. Konstantinov, K. Hatfield, I.V. Perminova, Nature-like solution for removal of direct brown 1 azo dye from aqueous phase using humics-modified silica gel, Chemosphere, 145 (2016) 83–88.

[20] C. Kannan, K. Muthuraja, M.R. Devi, Hazardous dyes removal from aqueous solution over mesoporous aluminophosphate with textural porosity by adsorption, J. Hazard. Mater., 244–245 (2013) 10–20.

[21] R.M. Garcia, R. Carleer, M. Arada Pérez, G. Gryglewicz, J. Maggen, T. Haeldermans, J. Yperman, Adsorption of Cibacron Yellow F-4G dye onto activated carbons obtained from peanut hull and rice husk: kinetics and equilibrium studies, Biomass Convers. Biorefin., (2020) 1–17, doi: 10.1007/s13399-020-00699-w.

[22] A. Mittal, R. Ahmad, I. Hasan, Poly(methyl methacrylate)-grafted alginate/Fe_3O_4 nanocomposite: synthesis and its application for the removal of heavy metal ions, Desal. Water Treat., 57 (2015) 19820–19833.

[23] Y. Yang, H. Liao, Z. Tong, C. Wang, Porous Ag/polymer composite microspheres for adsorption and catalytic degradation of organic dyes in aqueous solutions, Compos. Sci. Technol., 107 (2015) 137–144.

[24] I. Anastopoulos, I. Pashalidis, A.G. Orfanos, I.D. Manariotis, T. Tatarchuk, L. Sellaoui, A. Bonilla-Petriciolet, A. Mittal, A. Núñez-Delgado, Removal of caffeine, nicotine and amoxicillin

from (waste)waters by various adsorbents. A review, J. Environ. Manage., 261 (2020) 110236 (1–9), doi: 10.1016/j.jenvman.2020.110236.

[25] A. Mittal, L. Kurup, Column operations for the removal & recovery of a hazardous dye 'Acid Red-27' from aqueous solutions, using waste materials-bottom ash and de-oiled soya, Ecol. Environ. Conserv., 13 (2006) 181–186.

[26] M. Zhang, Y. Mao, W. Wang, S. Yang, Z. Song, X. Zhao, Coal fly ash/$CoFe_2O_4$ composites: a magnetic adsorbent for the removal of malachite green from aqueous solution, RSC Adv., 6 (2016) 93564–93574.

[27] M. Visa, A.M. Chelaru, Hydrothermally modified fly ash for heavy metals and dyes removal in advanced wastewater treatment, Appl. Surf. Sci., 303 (2014) 14–22.

[28] M. Gao, Q. Ma, Q. Lin, J. Chang, W. Bao, H. Ma, Combined modification of fly ash with $Ca(OH)_2$/Na_2FeO_4 and its adsorption of Methyl orange, Appl. Surf. Sci., 359 (2015) 323–330.

[29] S. Dash, H. Chaudhuri, G. Udayabhanua, A. Sarkar, Fabrication of inexpensive polyethylenimine-functionalized fly ash for highly enhanced adsorption of both cationic and anionic toxic dyes from water, Energy Fuel, 30 (2016) 6646–6653.

[30] S. Li, B. Li, L. Gong, L. Tang, Y. Feng, D. Jia, Y. Zhou, Hyperbranched polysiloxane for highly stretchable and tough hydrogel by one-pot in situ polymerization, J. Controlled Release, 259 (2017) E122–E122, doi: 10.1016/j.jconrel.2017.03.251.

[31] A.S. Fawcett, T.C. Hughes, L. Zepedavelazquez, M.A. Brook, Phototunable cross-linked polysiloxanes, Macromolecules, 48 (2015) 6499–6507.

[32] T. Zhang, B. Jiang, Y. Huang, Combined use of methacrylate/epoxy functionalized silanes for tuning of hyperbranched polysiloxane structure, Mater. Chem. Phys., 254 (2020) 123525 (1–8), doi: 10.1016/j.matchemphys.2020.123525.

[33] K. Indulekha, D. Thomas, N. Supriya, R.S. Rajeev, D. Mathew, K.N. Ninan, C. Gouri, Inherently flame retardant vinyl bearing hyperbranched polysiloxanes having improved thermal stability-Ceramization and analysis of associated thermal properties, Polym. Degrad. Stab., 147 (2018) 12–24.

[34] Y. Zheng, K.J. Thurecht, W. Wang, Polysiloxanes polymers with hyperbranched structure and multivinyl functionality, J. Polym. Sci. Polym. Chem., 50 (2012) 629–637.

[35] N. Xu, E.J. Stark, P.I. Carver, P. Sharps, J. Hu, C. Hartmann-Thompson, Hyperbranched polyhedral oligomeric silsesquioxane (HB-POSS) nanomaterials for high transmission and radiation-resistant space and solar applications, J. Appl. Polym. Sci., 130 (2013) 3849–3861.

[36] S. Soni, P.K. Bajpai, J. Mittal, C. Arora, Utilisation of cobalt doped iron based MOF for enhanced removal and recovery of methylene blue dye from waste water, J. Mol. Liq., 314 (2020) 113642 (1–12), doi: 10.1016/j.molliq.2020.113642.

[37] A. Witek-Krowiak, A. Dawiec, Removal of cationic dyes from aqueous solutions using microspherical particles of fly ash, Water Environ. Res., 84 (2012) 162–169.

[38] Uma, S. Banerjee, Y.C.J. Sharma, Equilibrium and kinetic studies for removal of malachite green from aqueous solution by a low cost activated carbon, Ind. Eng. Chem., 19 (2013) 1099–1105.

[39] L. Ai, H. Huang, Z. Chen, X. Wei, J. Jiang, Activated carbon/$CoFe_2O_4$ composites: facile synthesis, magnetic performance and their potential application for the removal of malachite green from water, Chem. Eng. J., 156 (2010) 243–249.

[40] S. Chowdhury, P. Saha, Sea shell powder as a new adsorbent to remove Basic Green 4 (malachite green) from aqueous solutions: equilibrium, kinetic and thermodynamic studies, Chem. Eng. J., 164 (2010) 168–177.

[41] J. Qin, F. Qiu, X. Rong, H. Zhao, D. Yang, J. Wan, Preparation of graphite oxide/polyurethane foam material and its removal application of malachite green from aqueous solution, J. Appl. Polym. Sci., 131 (2015) 8558–8572.

[42] F. Deniz, R.A. Kepekci, Bioremoval of Malachite green from water sample by forestry waste mixture as potential biosorbent, Microchem. J., 132 (2017) 172–178.

[43] F. Naseeruteen, H. Nsa, S. Fbm, N. Wsw, F.S. Mehamod, Adsorption of malachite green from aqueous solution by using novel chitosan ionic liquid beads, Int. J. Biol. Macromol., 107 (2018) 1270–1277.

[44] X. Li, Y. Zhang, L. Jing, X. He, Novel N-doped CNTs stabilized Cu_2O nanoparticles as adsorbent for enhancing removal of malachite green and tetrabromobisphenol A, Chem. Eng. J., 292 (2016) 326–339.

[45] H. Liu, L. Chen, J. Ding, Adsorption behavior of magnetic amino-functionalized metal-organic framework for cationic and anionic dyes from aqueous solution, RSC Adv., 6 (2016) 48884–48895.

[46] E. Sharifpour, H.Z. Khafri, M. Ghaedi, A. Asfaram, R. Jannesar, Isotherms and kinetic study of ultrasound-assisted adsorption of malachite green and Pb^{2+} ions from aqueous samples by copper sulfide nanorods loaded on activated carbon: experimental design optimization, Ultrason. Sonochem., 40 (2018) 373–382.